

# The structure of sea urchin spines, large biogenic single crystals of calcite

X. SU, S. KAMAT, A. H. HEUER

Department of Materials Science and Engineering, Case Western Reserve University,  
10900 Euclid Avenue, Cleveland, OH 44106, USA

E-mail: ahh@po.cwru.edu

Sea urchin spines are porous, single crystal Mg-rich calcite [(Mg, Ca)(CO<sub>3</sub>)] with a three dimensional meshwork architecture. The crystallographic orientation of large (~10 cm in length) spines from *Heterocentrotus trigonarius* was determined using the X-ray back-reflection Laue technique; the long axis of all spines is parallel to the (00·1) direction of calcite. The internal structure was studied using SEM and TEM. The macropore structure dominated the SEM images, whereas many small (~80 nm) protein occlusions can be observed within the single crystal spines using TEM. The spines appeared crystallographically perfect in the TEM. The bend strengths of a group of spines were also determined and varied between ~13 and 41 MPa. © 2000 Kluwer Academic Publishers

## 1. Introduction

Skeletal tissue in echinoderms is made up of Mg-rich calcite [(Mg,Ca)(CO<sub>3</sub>)]. In contrast to other invertebrates, hard tissue in echinoderms generally contains interconnecting cavities and much open space. Spines of sea urchins are particularly interesting; even though individual spines can be as long as tens of centimeters, they behave as single crystals when examined with polarized light or by X-rays. The interpretation of X-ray diffraction data has not been straightforward. Some [1–4] believe that each skeletal element of echinoderms are single crystals, while others [5, 6] suggest that each skeletal element is an aggregate of perfectly aligned crystallites.

The echinoderm skeleton is remarkably strong, considering the high porosity present. Weber *et al.* [7] and Currey [8] determined the crushing strength of the skeleton of several echinoid species. They showed that the strength to weight ratio of this type of hard tissue is comparable to or slightly lower than mollusc shells.

Pure calcite cleaves easily along {10·4} planes. However, the fracture surface of the skeletal tissue studied previously did not show any cleavage faces, in spite of the high mineral content (>99%); rather, the material fractured in a conchoidal manner. It has been proposed [9] that the proteins occluded within the skeleton during growth are responsible for the unusual mechanical properties of echinoderm skeletal tissue; in essence, their presence is thought to strengthen the skeleton and prevent it from cleaving in the same way as mineral calcite.

Sea urchins belong to one of the five classes of echinoderms\* [4, 5]. Their skeleton is made up of ten fused plates (“tests”) that encircle the body. Long, movable spines are connected to the skeleton via a “ball and socket” arrangement; these spines are their primary defense against predators. The spines are both long and strong, and can be up to 30 cm long and 1 cm thick. Such large samples are suitable for microstructural and mechanical property investigations.

Spines of *Heterocentrotus trigonarius* were used in this study (Fig. 1). Our analysis confirmed that the spines are large biogenic single crystals of Mg-rich calcite. The spines generally have two flat surfaces and assume an overall triangular or rectangular cross-section; the crystallographic orientation of the flat faces of 45 spines was determined for the first time and is reported here. In addition, we used both scanning electron microscopy (SEM) and transmission electron microscopy (TEM) to study the microarchitecture and microstructure of the spines. Finally, we determined the bend strength of a group of representative spines.

## 2. Experimental procedure and results

Adult spines of *H. trigonarius* (Fig. 1a<sup>†</sup>) from the Marshall Islands in the South Pacific were provided by Dr. Rich Mooi of the California Academy of Science. The spines are purple in color, and in cross-section have at least two flat sides connected by one or two curved sides (Fig. 1b). The angles between the two flat faces vary from spine to spine; some are smaller than 90° (the

\*The term Echinoderm means “spiny-skinned”. Echinoderms are considered the most advanced invertebrates, and are classified closest to the vertebrates. The five classes are sea urchins, sea lillies, sea stars, brittle stars and sea cucumbers.

<sup>†</sup>The sea urchin for Fig. 1a was kindly provided by Dr. Cynthia Ahearn of the National Museum of Natural History.

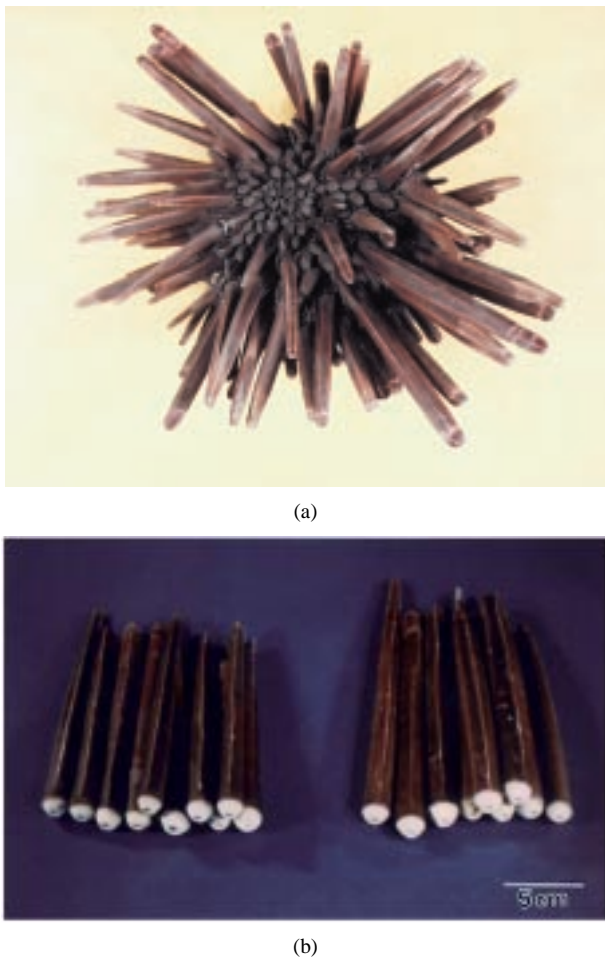


Figure 1 (a) Sea urchin *H. trigonarius*; (b) Spines of *H. trigonarius*. The spines have two flat faces; the angles between the two flat faces in the left hand group is less than  $90^\circ$ , while in the right hand group, this angle is greater than  $90^\circ$ .

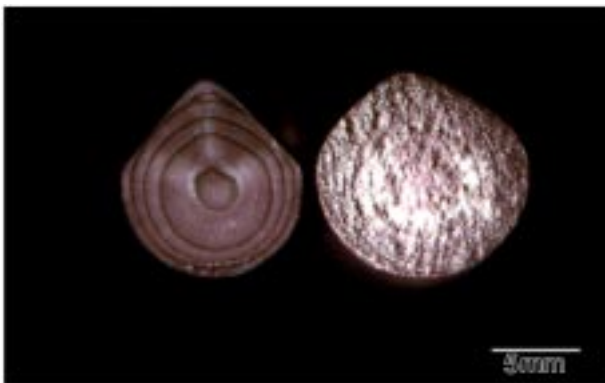


Figure 2 Cross-sectional view of two spines of *H. trigonarius*. The angle between the two slightly polished flat faces of the left hand sample is less than  $90^\circ$ , while this angle in the right hand (fractured) sample is greater than  $90^\circ$ .

left hand group of Fig. 1b) while others are greater than  $90^\circ$  (the right hand group of Fig. 1b). Spines 5 to 15 cm long were used in this study.

X-ray Laue back reflection photographs (Cu radiation) were used to identify the crystallographic orientation of a group of spines. For this, either whole spines or  $\sim 1$  cm long section of spines were used. In the left hand sample of Fig. 2, the two vertical flat surfaces were lightly polished, as well as the surface normal to

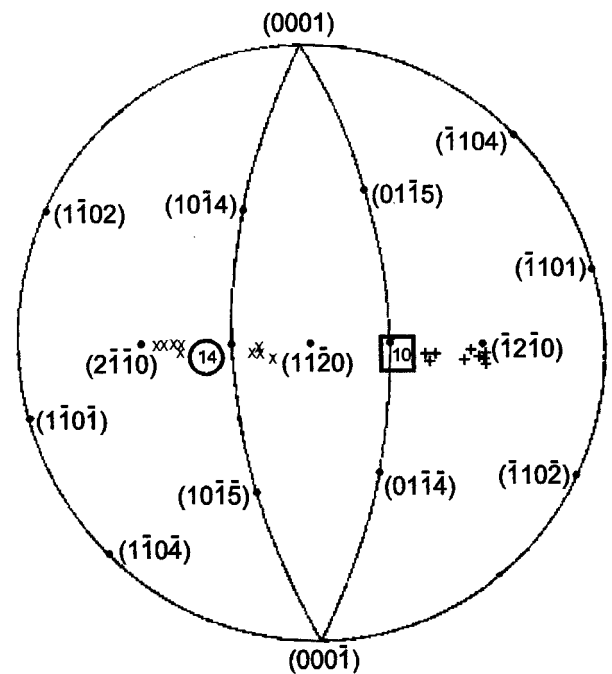


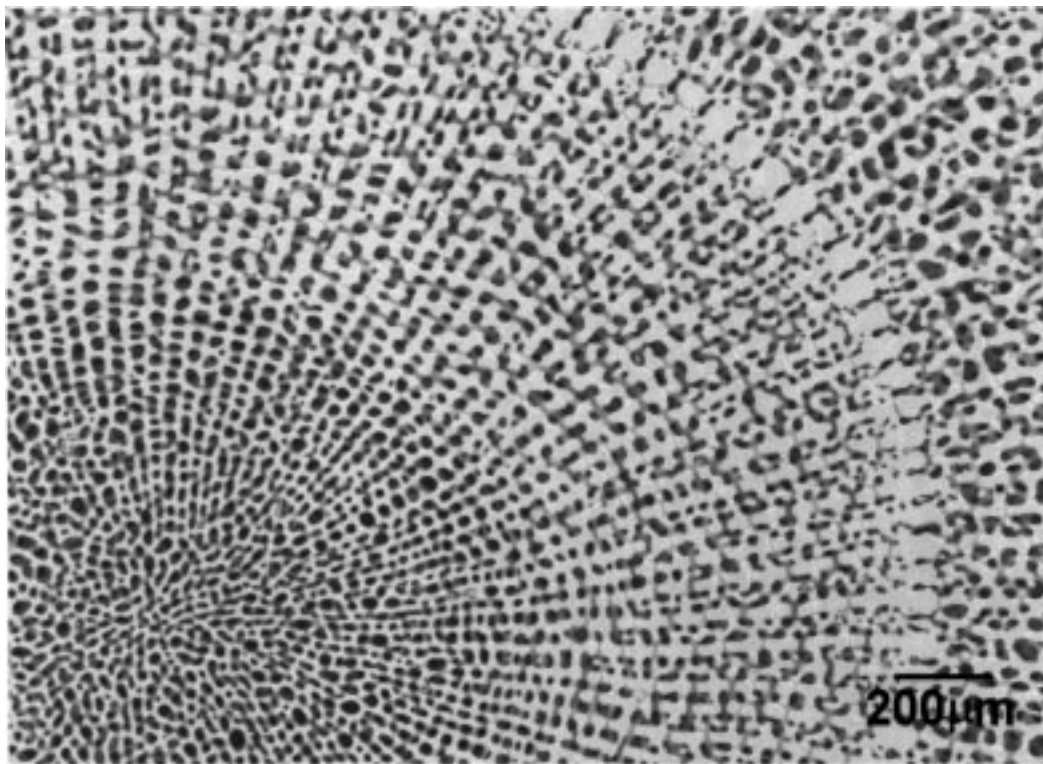
Figure 3 Stereographic projection of the crystallographic orientations of the two flat faces of a group of spines determined by Laue back-reflection photographs. The plane normals of the left hand faces are indicated by an "x", whereas the plane normals of the right hand faces are indicated by a "plus". The number in the circle is the number of spines having that common orientation of the left-hand faces, while the number in the square are those having that common orientation of the right-hand faces.

the spine axis, and back reflection photographs taken of the three surfaces. A small portion of this spine was powdered using an agate mortar and pestle so the lattice parameters could be determined by standard X-ray means; these data were necessary to accurately plot the stereographic projection of Fig. 3.

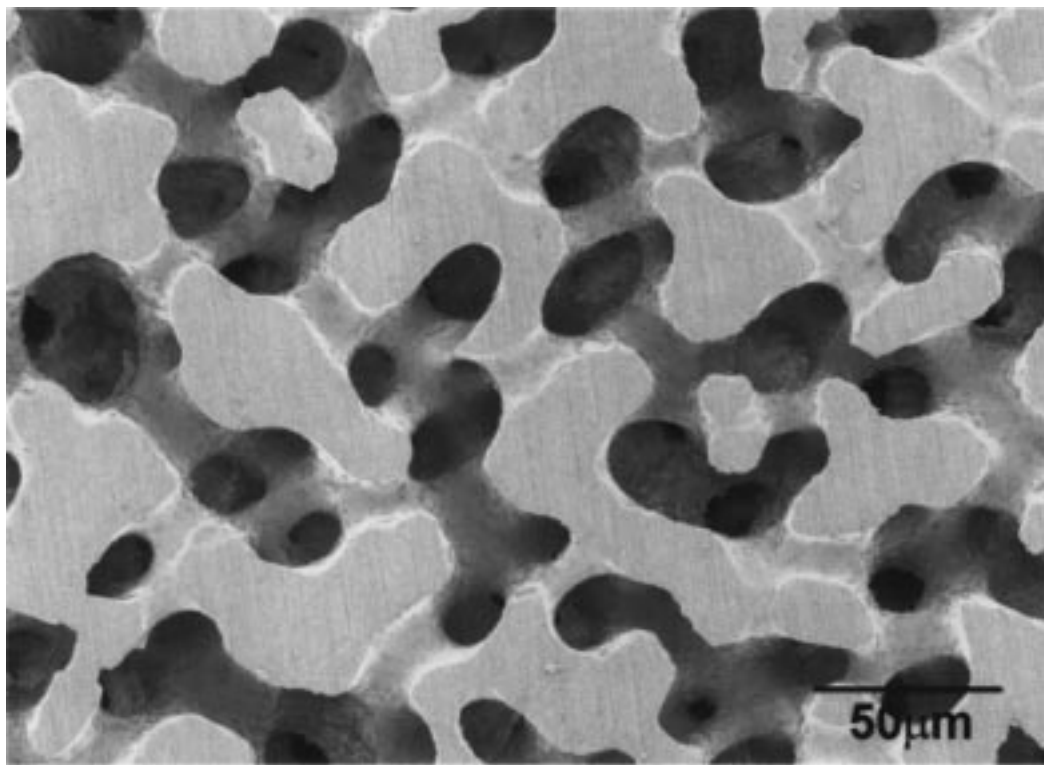
About 1 g of the powdered sample was mixed with an equal quantity of  $\alpha$ - $\text{Al}_2\text{O}_3$ , and an XRD powder pattern taken with Ni-filtered Cu  $K_\alpha$  radiation. A Nelson-Riley plot, using  $\text{Al}_2\text{O}_3$  as the internal standard, gave the  $c$  and  $a$  lattice parameters as 16.919  $\text{\AA}$  and 4.943  $\text{\AA}$ , respectively. Conventional X-ray diffraction spectra from cross-sections of spine samples (not shown here), also using Ni-filtered Cu  $K_\alpha$  radiation, revealed a single (00-6) peak of calcite, indicating that the long axes of the spines were parallel to the  $c$  axis of calcite. This result is consistent with previous data [1, 3, 5].

We have examined in detail the single crystal character of 45 spines which had two nearly flat faces meeting at an angle near  $90^\circ$ . Of this group, 25 had interfacial angles less than  $90^\circ$  (the sample on the left in Fig. 2 has the flat faces meeting at  $\sim 80^\circ$ ), while 20 spines had interfacial angles greater than  $90^\circ$  (the sample on the right in Fig. 2). Laue photographs were taken from both types of spines but there was no correlation with the crystallographic orientation of the faces, as will be discussed next.

The orientations determined from the Laue photographs are shown in Fig. 3. Referring to the orientation of the spines shown in Fig. 2, the plane normals of the left hand faces are indicated by an "x", whereas the plane normals of the right hand faces are indicated by a "plus". For the left hand orientation, none had



(a)



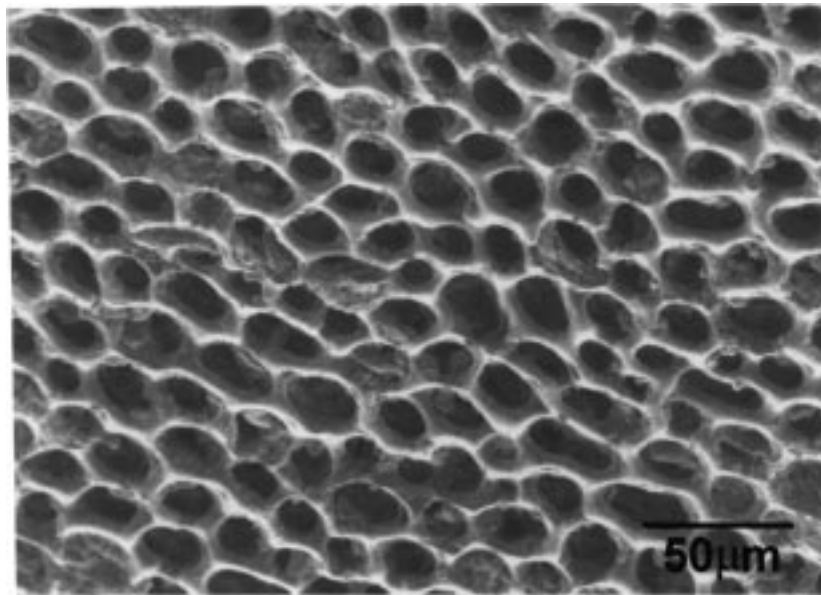
(b)

Figure 4 (a) Cross-sectional SEM image taken from the center of a spine; (b) SEM image of a spine that has been partially decalcified with EDTA. The thick band in (a) shows one of the growth rings of the spine.

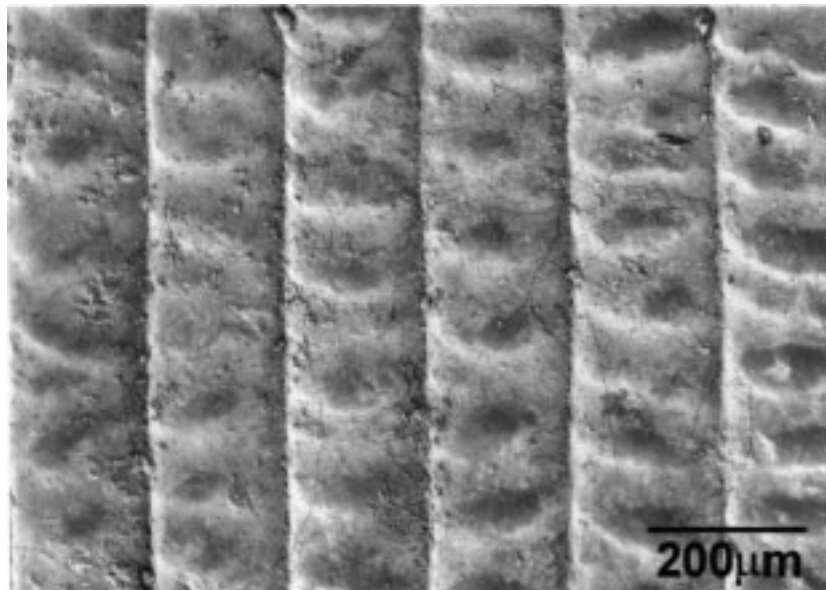
a low index form—all faces were of the type  $\{hk\cdot 0\}$ , although 14 had a common orientation,  $\sim\{5\bar{1}\cdot 0\}$ . The right hand faces tended to be more crystallographic. 10 spines had a face normal approximately parallel to  $\langle 01\cdot 0\rangle$ , while 6 were approximately parallel to  $\langle \bar{1}2\cdot 0\rangle$ . Several spines showed Laue patterns sufficiently far from a low index zone that the patterns could not be

solved; nevertheless, we believe that these spines also had their long axes parallel to  $\langle 00\cdot 1\rangle$ . It is clear that the spines are, to all intents and purposes, perfect single crystals of calcite.

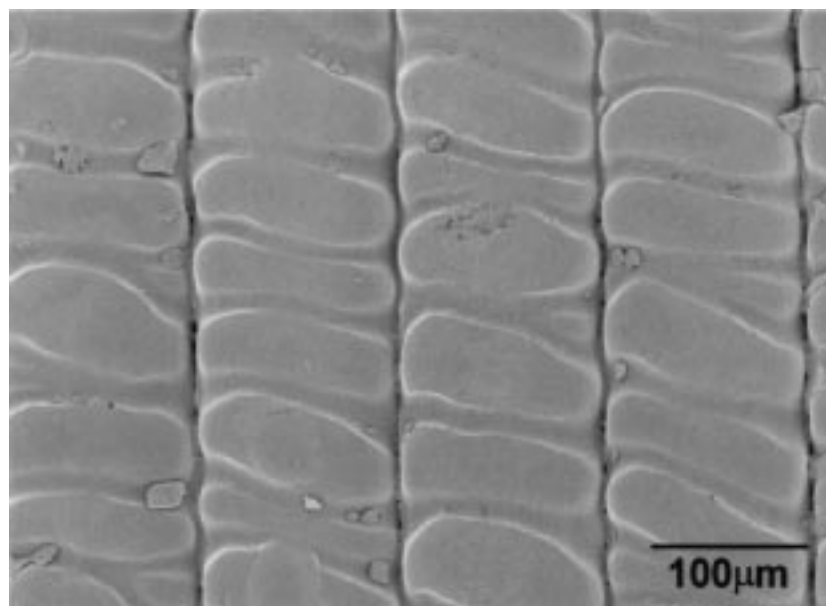
Both cross-sectional and longitudinal samples were used for SEM examination. For this, portions of spines were sectioned with an Isomet 11-1180 Low Speed



(a)

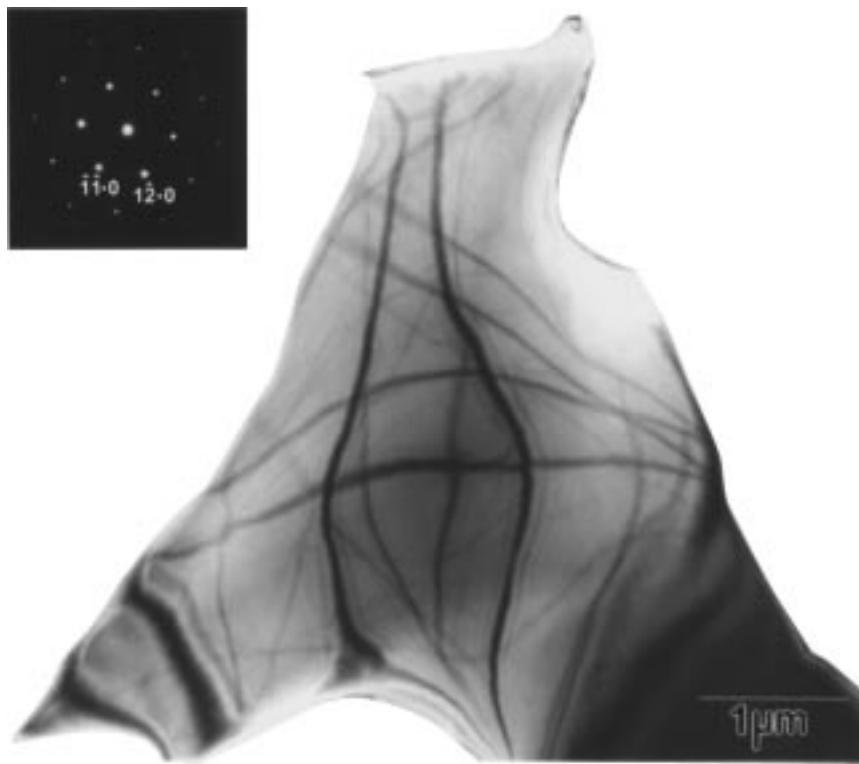


(b)

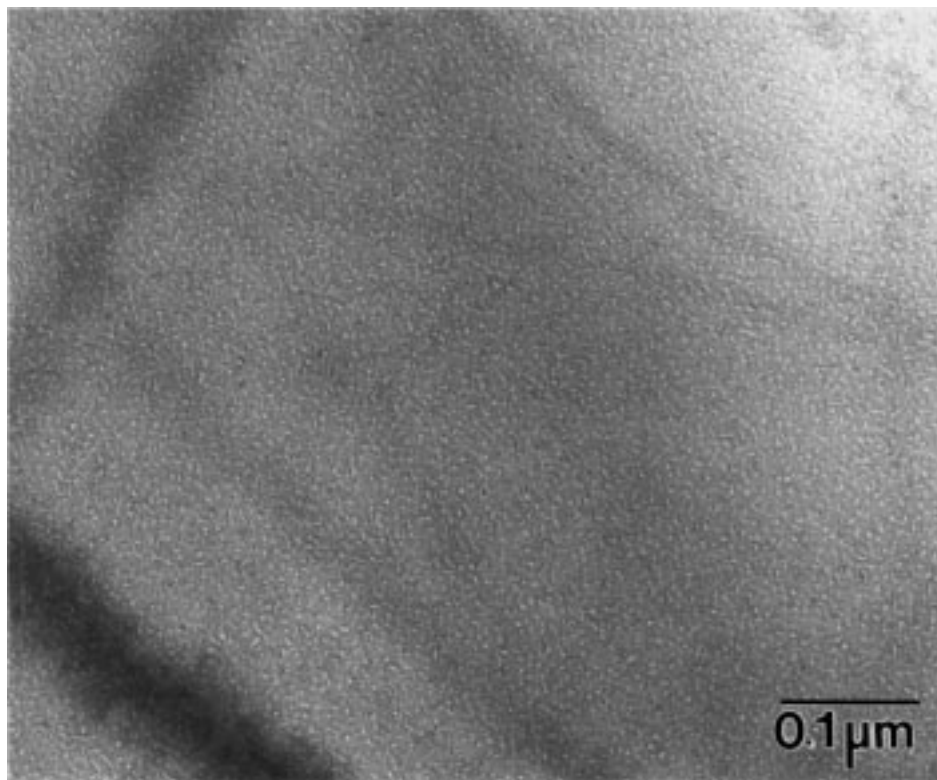


(c)

*Figure 5* SEM images of the surface of a spine, (a) is from the white-colored region (the “socket” region), while (b) shows a portion of the purple cuticle that is present on the vertical surface of the spine, (c) shows the vertical surface after dissolving the cuticle in sodium hypochlorite.



(a)



(b)

*Figure 6* (a) TEM image of a thin foil sectioned nearly perpendicular to a spine axis. The inset is a selected area diffraction pattern, after modest tilting to the (00-1) zone axis. (b) TEM image showing protein occlusions within a spine; they are  $\sim 80$  nm in diameter.

Saw (Buehler, Lake Bluff, IL) fitted with a diamond blade, and two orthogonal surfaces of each section (one normal to the spine axis) were polished using 600, 1200 and 2400 grit SiC paper followed by  $3 \mu\text{m}$  diamond abrasive. One set of samples was briefly demineralized with ethylenediaminetetraacetic acid (EDTA—a Ca ion chelator) and the other set treated with sodium

hypochlorite. Both sets of samples were then dehydrated in graded ethanol and were coated with 10 nm carbon and observed in a Hitachi-S4500 FEG SEM operating at 2 kV.

The polished sample in Fig. 2 suggests that the spines grow in a layered fashion, and details of the layered structure are clearly revealed by SEM. Fig. 4a is taken

from the center of a spine cross section. The three-dimensional meshwork of the spines is clearly revealed, in agreement with earlier reports [5]. In the biological literature [10], the mesh is termed a *stereom*, the individual skeletal struts being referred as *trabeculae*. Fig. 4a reveals that the spine cross-section is divided homogeneously by radiating trabeculae which have an average intertrabecular angle of  $3.2^\circ$ . The thickness of the trabeculae is about  $10\ \mu\text{m}$  in the center and  $26\ \mu\text{m}$  at the edge. The distance between adjacent radiating trabeculae increases from the center to the edge. Thinner trabeculae connect two adjacent radiating trabeculae and have an average thickness of  $14\ \mu\text{m}$ .

Fig. 4a reveals that considerable porosity is distributed within the spine; the pore dimensions are uniform in the spine, except in the very center (the mean pore diameter is  $28 \pm 16\ \mu\text{m}$  in the center and  $35 \pm 17\ \mu\text{m}$  in other regions). The growth rings visible in the hand section (Fig. 2) are the thick bands seen in SEM and are parallel to the outer surface of the spine. The radiating trabeculae are well aligned on either side of the growth rings.

Neither polished specimens nor those etched with either sodium hypochlorite or EDTA revealed grain boundaries. Fig. 4b is cross-sectional micrograph of a sample partially decalcified with EDTA. The surface is smooth and all the trabeculae are continuous. These results again support the single crystal hypothesis. During the SEM examination, we measured the Mg/Ca ratio using EDS, and found that the spines contain  $\sim 7\ \text{mol. \% MgCO}_3$ .

We also examined the surface of the spines in the SEM. The “socket” surface is very porous, Fig. 5a. However, the purple cuticle covering the spine surface is continuous (Fig. 5b). The hard tissue under the cuticle can be revealed by dissolving the cuticle in sodium hypochlorite. The vertical trabeculae are clearly revealed (Fig. 5c) and show that the external spine surface is essentially devoid of porosity, other than that on the socket surface.

The microstructure of the spines was studied at higher magnification in the TEM (Fig. 6a). For this, TEM thin foils were prepared from thin petrographic thin sections cut normal to the spine axis using conventional ion thinning; they were studied in a Philips CM 20 TEM operating at 200 kV. The inset in Fig. 6a is a selected area diffraction (SAD) pattern of the sample after tilting to the closest zone axis. The SAD data confirms that the long axis of the spine is parallel to  $\langle 00\cdot 1 \rangle$  of calcite. No grain boundaries can be observed in this image, nor in any of the electron transparent material we have studied. Under weakly diffracting conditions, Fig. 6b, irregular protein occlusions  $78 \pm 37\ \text{nm}$  in diameter, can be clearly seen. They exist as isolated islands within the hard tissue and do not appear to be interconnected.

The flexural strength of a group of spines were tested using specimens that had two nearly parallel surfaces, so they could be tested in the as-received condition. Their widths ranged from 9.4 to 12 mm, while the depths varied from 8.9 to 11.9 mm. Four point bend

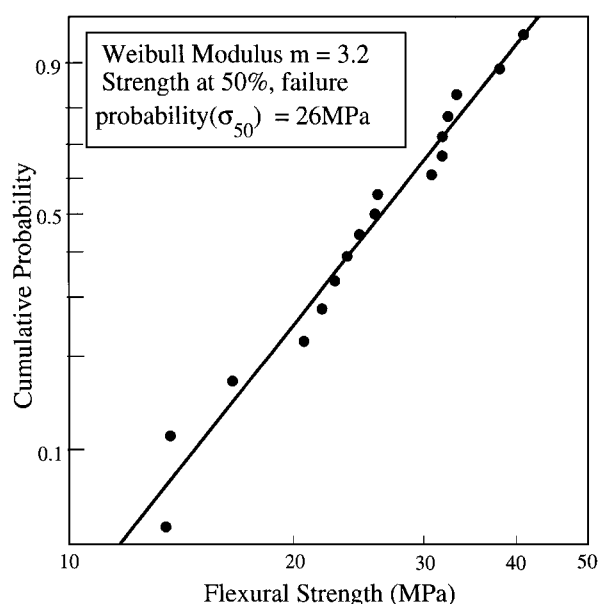


Figure 7 Weibull plot of the bend strength of 17 spines measured in four-point bending.

tests were conducted with outer and inner load point spans of 30 mm and 15 mm, respectively, and a cross head speed of 0.1 mm/min.

The strength of 17 spines is shown in the Weibull plot of Fig. 7; the average strength ( $\sigma_{50}$ ) is 26 MPa, and the Weibull modulus is rather low, 3.2. (For comparison, the reported compressive strength of spines of another sea urchin species, *H. mammillatus* is 48 MPa [8]). The flexural strength is about 40% that of dense biogenic  $\text{CaCO}_3$ , such as the aragonitic shells of the conch *Strombus Gigas* (56 MPa) [11], and is impressive given the highly porous nature of the spines.

The right hand sample in Fig. 2 is a fractured spine. The fracture surface of this sample is shown at higher magnification in the SEM images in Fig. 8a and b; the surface morphology is remarkably similar to the polished surfaces, Fig. 4a and b. The fracture was clearly brittle and cleavage-like, the cracks propagating along the basal plane of calcite.  $\langle 00\cdot 1 \rangle$  is not normally a cleavage plane in calcite.

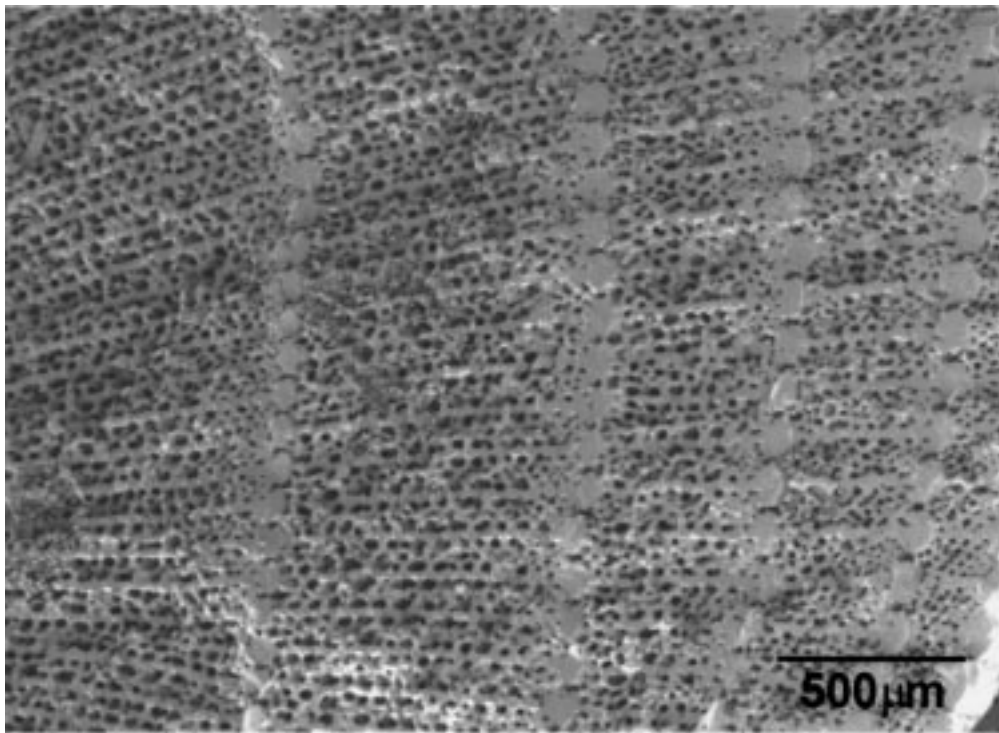
Lastly, we have isolated the “matrix” (the biological term for organic matter in mineralized tissue) from the spines; it is present at 0.26 wt. %. Unfortunately, attempts at protein analysis were unsuccessful, undoubtedly due to degradation of the organic matter in the spines; in fact, these samples were collected  $\sim 50$  years ago [12]. We are in the process of obtaining fresh spines from *H. trigonarius* to characterize the proteins.

### 3. Conclusion

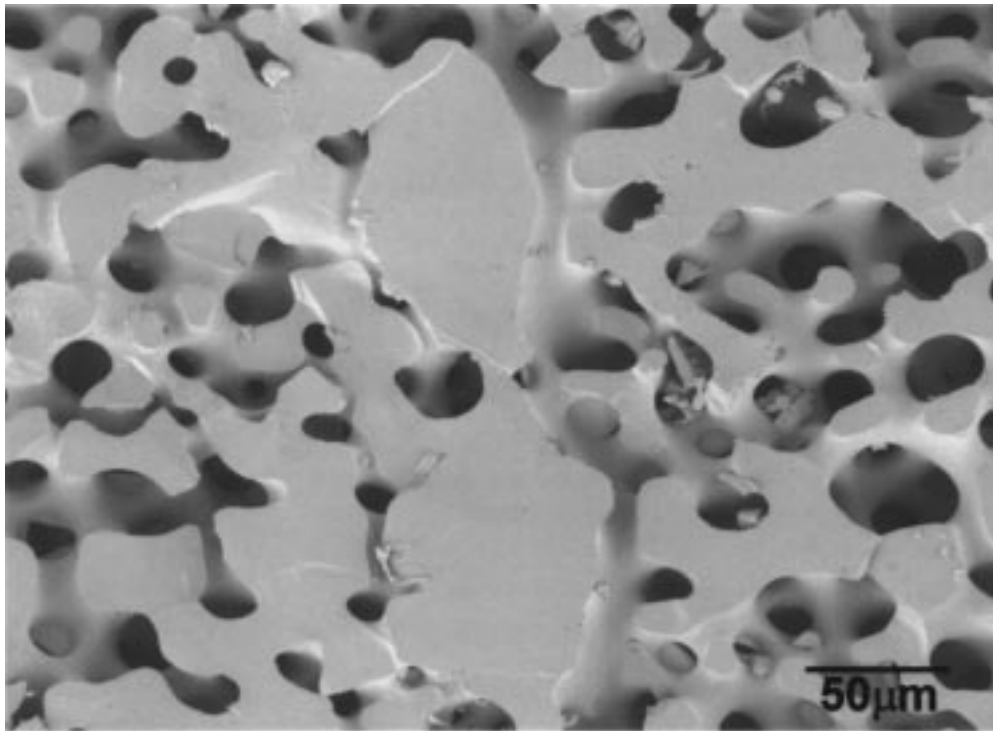
Each spine of *H. trigonarius* is a large porous calcite single crystal, whose long axis is parallel to  $\langle 00\cdot 1 \rangle$ . They contain irregular protein occlusions in the form of small vesicles,  $\sim 80\ \text{nm}$  in diameter. The bend strength of the spines vary from 13 to 41 MPa.

### Acknowledgement

The research was supported by EPRI.



(a)



(b)

Figure 8 SEM images of the fracture surface of a bend sample. See text for further discussion.

## References

1. C. D. WEST, *J. Paleontol* **11** (1937) 458.
2. D. NICHOLS and J. D. Currey, in "Cell Structure and Its Interpretation," edited by S. M. McGee-Russell and K. F. A. Ross (Arnold, London, 1968) p. 251.
3. G. DONNAY and D. L. PAWSON, *Science* **166** (1969) 1147.
4. D. NICHOLS, "Echinoderms" (Hutchinson, London, 1969) p. 123.
5. D. M. RAUP, in "Physiology of Echinodermata," edited by R. A. Booloootian (Wiley, New York, 1966) p. 379.
6. P. L. O'NEIL, *Science* **213** (1981) 646.
7. W. J. WEBER, R. GREER, B. VOIGHT, E. WHITE and R. ROY, *Journal of Ultrastructure Research* **26** (1969) 355.
8. J. D. CURREY, *J. Mar. Biol. Ass. U. K.* **55** (1975) 419.
9. A. BERMAN, L. ADDADI and S. WEINER, *Nature* **331** (1988) 546.
10. A. B. SMITH, in "Skeletal Biomineralization: Patterns Processes and Evolutionary Trends," edited by J. G. Carter (Van Nostrand Reinhold, New York, 1990) p. 413.
11. L. T. KUHN-SPEARING, H. KESSLER, E. CHATEAU, R. BALLARINI and A. H. HEUER, *Journal of Materials Science* **31** (1996) 6583.
12. R. MOOI, private communication.

Received 16 November 1999  
and accepted 6 March 2000